Responses to referee comments

We are grateful to both referees for their constructive and helpful comments on our manuscript. Below we respond point-by-point to the comments and list the changes made to the manuscript.

Referee 1 Malcom Levitt:

1) In the abstract, it is not very clear that the confining cage is not C60 but an open-cage variant (in fact two variants) of C60.

Response: The first sentence of the abstract has been rephrased:
"… confined in two different modified open C_{60} derived cages are determined."
Further changes have been made in reply to Referee 2, 1).

2) In the introduction, references are given to some of the molecular endofullerenes produced by the Kyoto group and others, but some important systems of this kind are omitted, for example the water endofullerene (Murata and coworkers) and also the HF and CH4 endofullerenes (Whitby and coworkers).

Response: Three additional references have been included:
a) K. Kurotobi and Y. Murata, Science, 2011, 333, 613–616 ($H_2O@C_{60}$)
b) A Krachmalnicoff *et al*., Nature Chemistry, 2016, 8(10) 953–957 ($HF@C_{60}$)
c) S Bloodworth *et al*., Ang. Chem. Int. Ed., 2019, 58(15) 5038–5043 ($CH_4O@C_{60}$)

3) The ball and stick graphics in Fig.1 do not depict the chemical structures of these compounds clearly enough. They should be supplemented by ChemDraw-style line structures showing clearly the chemical nature of the orifice and the appended groups.

Response: Fig. 1 has been changed to display only NO@C60-OH1 with the left part as "side view" of the modified C_{60} cage represented by true balls-and-sticks together with the caged NO represented by van-der-Waals spheres. The right part now shows a "top view" onto the orifice with the orifice atoms represented by van-der-Waals spheres. The caged NO again is also displayed as van-der-Waals spheres, but the modified C_{60} cage represented only by sticks. NO@C60-OH3 is now shown as Fig. A1 in the appendix identical to the original Fig. 1b).

4) There are a few places where I felt that more references would be appropriate, especially for readers who are not highly conversant with EPR techniques. For example the PEANUT method is not referenced. No reference is given for the lambda value for NO (line after Eq.1). No explicit reference is given for the reported data on related systems (end of first paragraph on page 7).

Response: References had been misplaced at several instances and are given now at the appropriate places.

5) It is not clear until quite late in the discussion that the hyperfine data refers to coupling to the 14N nucleus.

Response: This has been clarified by replacing the sentence starting at line 150 (<u>now line 165</u>) by:
"The frequency position at the low field side of the spectrum and the magnitude of the shift is inconsistent with proton hfi but is indicative for a dominant dipolar ^{14}N hfi, …".

6) A comparison with the observations reported on the similar O2 system (Futagoishi et al.) would have been interesting and enhance the manuscript.

Response: This has been incorporated at line 99 after "… (200 K) is determined" (<u>now line 108</u>) by:
"The lifting of $^2\pi_x/^2\pi_y$ degeneracy is not unexpected considering the observation of a finite zero-field-splitting for $^3O_2$ in a cage with C_1 symmetry (Futagoishi et al., 2017). In this study the potential barrier for librational motions of $^3O_2$ was estimated as 398 cm^{-1}, by measuring the shift of its principal ZFS component with respect to the value of the free molecule. The size of this potential barrier is of the same order of magnitude as the one calculated for NO."

Referee 2:

1) The abstract needs some re-writing, compared to the clarity of the paper itself the abstract seems confusing, at least to me.

Response: The abstract has been modified for clarification (see also Ref 1, 1)).

2) At the end of the introduction, the authors state that a smaller g3-value "deduced by an analysis of a CW measurement, necessitated confirmation by pulse ESR experiments, better suited for the study of very broad spectra." I would challenge this view of the difference in CW EPR and pulse EPR data content. In the case described here, the g3 value of 0.2 (instead of 0.7 reported now in this paper) was deduced by fitting CW EPR spectra (if I understood correctly). In a way, ESE-detected EPR has a built in T2-filter that simplifies the spectra (reducing the broadness of the high-field region). I think the authors should point that out, as this is the real original point they have made here (or, if they think this is wrong, explain, why pulse EPR may be better suited).

Response: The referee is quite right in his remark that because of possible T_2 variations in the spectral range the true absorption line shape can be distorted in an FSE spectrum. However, we disagree with the referee about a "simplification", i.e. complete loss of the extreme high-field part, of the spectrum suggested to exist for $g_3 = 0.225$ in the FSE spectra. The T_2 determined by a 2-pulse echo sequence does not show any significant shortening towards the high-field end of the observed FSE spectrum, instead T_2 increases at temperature used for the FSE spectra with increasing field. Furthermore, the FSE spectrum shows a clear high-field shoulder which is however much too broad for being picked up by typically achievable B_0 modulation amplitudes. In addition we would like to point out that $g_3 = 0.225$ corresponds to B_0 beyond 3 T, while the cw spectra were recorded only up to 1.5 T. For clarification, a sentence has been added to the introduction at line 26 after "… very broad spectra" (now line 29):

"Although a T_2 variation as function of the external field can distort the shape of a pulse derived spectrum to some extent, difficulties in detecting extremely broad spectra with virtually absent changes within the typically achievable B_0 modulation amplitudes in cw ESR can lead to misinterpretations, in particular if the suggested spectrum extends a factor of two beyond the possible acquisition range."

In consequence, we have deleted the sentence starting "The FSE technique, …" on line 68 (now lines 76/77).

3) Figure 1 clearly needs to be amended with a chemical structure of the cage molecules - the DFT structures should also be shown from a side view, not only the top view.

Response 3): Figure 1 has been modified (see Referee 1, 3)).

4) *Figure 4 (PEANUT): the authors should explain the three black lines in the graph.*

Response: Figure and caption have been modified. The corresponding sentence in the caption no reads:

"The dashed vertical lines indicate the expected nutation frequency distributions (Stoll et al., 1998) at the three principal *g* values for NO@C60-OH3 in Table 1 (X band)."

5) *Last line on page 6:"level splitting" instead of "spitting":* Thank you for spotting (corrected).

6) Figs. 5 and 6 should be combined in one figure as a) and b) or Fig 6 should be moved into the SI. Again Figs 7 and 8 should be combined into one figure as a) and b).

Response: Figures 5 and 6 as well as Figs. 7 and 8 have been combined in one figure, respectively. We also have combined Figs. 2 and 3 as well as Figs. A1 and A2 into one figure, respectively. Correspondingly, figures have been renamed: Figs. 2, 3 are now Fig. 2, Fig. 4 is Fig. 3, Figs. 5, 6 are Fig. 4, Figs. 7, 8 are Fig. 5, and Figs. A1, A2 are Fig. A2. However, we would like to point out that Figs. 2, 4, 5, and A2 should be set spanning both columns in the final two column layout of the manuscript.

7) Page 10, beginning of 3.2: Would the authors expect a better resolution at intermediate field values when the frequencies for the ENDOR experiments are varied (through changes in g-strain?)?

Response: Best resolution is expected for van Hove orientations since in our case *g* matrix axes and hfi axes are expected to be collinear. This is true irrespective of the mw frequency used. For arbitrary orientations it is expected that at 34 GHz a better resolution in ENDOR would be obtained. The corresponding field range, however, was inaccessible for us due to low *g* values of interest here.

8) Figures 9, 10, 11: While I am usually all for original presentation of data, in this case I just think that plotting the three spectra in three rows above each other in Fig. 9 (without additional 3-D shift) would make it easier to see the "evolution" of orientation-dependent spectra. Then, Figs. 10 (and 11, I believe) could also be included in this figure.

Response: We prefer to keep the presentation of Fig. 9, however, have combined it with Fig. 10, but keep Fig. 11 separate. Figs. 9, 10 are now Fig. 6, and Fig. 11 is Fig. 7. Again, we would like to point out that Fig. 6 should be set spanning both columns in the final two column layout of the manuscript.

Further changes have been made to correct mistakes and to improve the manuscript.

The T_2 values given have been corrected by a factor of 2 (corrections in Figs. 4R, 5L). However, this has no impact on the results since the T_2 value have not been interpreted, but only their temperature dependence. The exponential fitting of the temperature dependence remains unaffected. The estimation of libration mode energies (now line 157) has been rephrased and another factor of 2 has been corrected. This again does not change any conclusion since the estimated value is off by an order of magnitude from the experimental observation.

The order of sentences has been changed at some instances to improve readability.

In Fig. 5 left, we have exchanged the 12.5 K data against 10 K data since the T_2 fits are significantly more stable due to the better S/N at this temperature.

A manuscript with all changes highlighted in blue is attached.

EPR Study of NO radicals encased in modified open C60 Fullerenes

Klaus-Peter Dinse[1], Tatsuhisa Kato[2], Shota Hasegawa[2], Yoshifumi Hashikawa[2], Yasujiro Murata[2], and Robert Bittl[1]

[1]Freie Universität Berlin, Fachbereich Physik, Arnimallee 14, 14195 Berlin, Germany
[2]Institute for Chemical Research, Kyoto University, Uji, Kyoto 611-0011, Japan

Correspondence: Robert Bittl (robert.bittl@fu-berlin.de)

Abstract. Using pulsed EPR techniques, the low temperature magnetic properties of the NO radical being confined in two different modified open C_{60}-derived cages are determined. It is found that the smallest principal g value g_3, being assigned to the axis of the radical, deviates strongly from the free electron value. This behaviour results from partial compensation of the spin and orbital contributions to the g_3 value. The measured g_3 values in the range of 0.7 yield information about the deviation of the locking potential for the encaged NO from axial symmetry. The estimated 17 meV asymmetry is quite small compared to the situation found for the same radical in polycrystalline or amorphous matrices ranging from 300 to 500 meV. The analysis of the temperature dependence of spin relaxation times resulted in an activation temperature of about 3 K, assigned to temperature activated motion of the NO within the modified open C_{60} derived cages with coupled rotational and translational degrees of freedom in a complicated 3-dimensional locking potential.

1 Introduction

In a series of recent publications, the Kyoto group has shown that it is possible to encapsulate small and even reactive molecules in a modified C_{60} cage with tailored entrance and exit holes (Hasegawa et al., 2018a; Futagoishi et al., 2017; Hashikawa et al., 2018). Using such designer type open cages instead of closed structures creates a new route for the preparation of interesting compounds. The family of endohedral fullerenes having closed carbon cages like N@C_{60} (Murphy et al., 1996), He@C_{60} (Saunders et al., 1994), H_2@C_{60} (Komatsu et al., 2005), H_2O@C_{60} (Kurotobi and Murata, 2011), HF@C_{60} (Krachmalnicoff et al., 2016), and CH_4@C_{60} (Bloodworth et al., 2019), as well as C_{82} (Stevenson et al., 1999) based metallo-endohedrals can thus be expanded significantly. It has been shown that these new compounds can be stable under ambient conditions, allowing easy handling. If encapsulated molecules are paramagnetic, as in case of $^3O_2$ or ^{2}NO, EPR is the method of choice for elucidating their properties. This allows determining not only the stationary spin Hamilton parameters but furthermore allows detecting of dynamic properties arising from internal dynamics or motion of the compound as a whole. In case of La@C_{82} for instance it was possible to conclude from an analysis of 2D EXCSY spectra that the metal ion is rigidly locked to the inside surface of the carbon cage (Rübsam et al., 1996). In the present case of encapsulated NO radical it was concluded

from the broad variance of its principal g matrix values (Hasegawa et al., 2018a) that even at low temperatures the radical is not fixed to a particular site. It was remarkable that the very small value quoted for the axial component (Hasegawa et al., 2018a) of 0.225 deviates significantly from the value determined for NO radicals trapped in a single crystal host (Ryzhkov and Toscano, 2005), or NO radicals adsorbed in zeolites (Poeppl et al., 2000). This very small value of g_3 = 0.225, deduced by an analysis of a cw measurement, necessitated confirmation by pulse EPR experiments, better suited for the study of very broad spectra. Although a T_2 variation as function of the external field can distort the shape of a pulse derived spectrum to some extent, difficulties in detecting extremely broad spectra with virtually absent changes within the typically achievable B_0 modulation amplitudes in cw EPR can lead to misinterpretations, in particular if the supposed spectrum extends a factor of two beyond the possible acquisition range. So far, neither relaxation nor nitrogen hyperfine data were reported, which might be important for a full characterization of the compound. It was the aim of the present study to obtain by multi-frequency EPR and ENDOR techniques a complete spin Hamiltonian parameter set for the encapsulated radical. In addition, the anticipated effects of a non-spherical cage potential on the radical are explored and effects due to the structural modification of the cage are studied.

2 Experimental Part

2.1 Sample Preparation

NO radicals trapped in two slightly different modified C_{60} cages, $C_{82}H_{28}N_3O_5S$ and $C_{82}H_{32}N_3O_5S$, were studied, in the following abbreviated by NO@C60-OH1 and NO@C60-OH3, respectively (see Fig. 1 for NO@C60-OH1 and Fig. A1 for NO@C60-OH3). The notation indicates the two different orifices with one and three OH groups, respectively. NO@C60-OH1 was prepared as described in reference (Hasegawa et al., 2018a) and NO@C60-OH3 combining the procedures described in references (Hashikawa et al., 2018; Hasegawa et al., 2018a). NO@C60-OH1 and NO@C60-OH3 were dissolved in CS_2 in 2.5 and 10 mM concentrations and sealed in quartz tubes for EPR spectroscopy.

2.2 EPR Spectroscopy

For pulsed EPR and ENDOR measurements at S and X band mw frequencies (3.4 and 9.8 GHz), various setups were employed. Echo-detected 9.8 GHz EPR measurements at low temperatures were conducted on Bruker ElexSys E580 and E680 instruments equipped with Oxford CF935 helium cryostats using Bruker MD4 Flexline ENDOR probe heads. Field swept Echo-detected EPR spectra (FSE) at 9.8 GHz were recorded using a two pulse "Hahn-echo" sequence (20-300-40 ns) at temperature of 3.6 to 12 K, yielding absorption type spectra. Transient nutation measurements at 9.8 GHz were conducted applying a PEANUT (Stoll et al., 1998) pulse sequence with a $\pi/2$ pulse length of 8 ns, a delay time τ of 130 ns and a high turning angle (HTAx) pulse of 4096 ns. Phase inversion time within the high turning angle (HTAx) pulse was incremented by 2 ns starting with an initial inversion after 16 ns. ENDOR spectra were recorded applying either a Mims pulse sequence with $\pi/2$ pulses of 20 ns, delay time τ of 200 ns and a rf π pulse length of 15 μs, or a Davies pulse sequence with pulse settings 40-30000-20-200 ns and

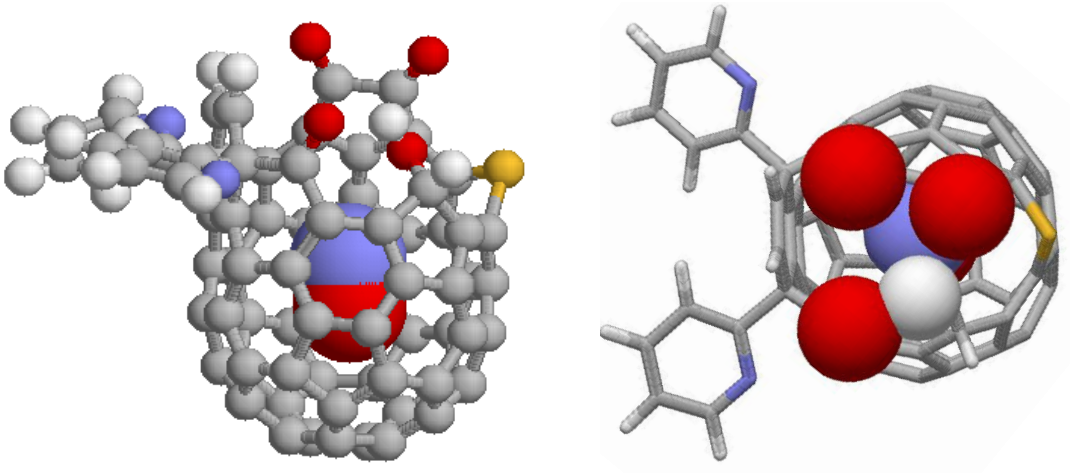

Figure 1. DFT optimized structure of NO@C60-OH1 with N "up". **Left:** Ball-and-stick representation of the modified C_{60} cage and van-der-Waals spheres of the caged NO with carbon (grey), hydrogen (white), nitrogen (blue), oxygen (red), and sulfur (yellow). **Right:** Top view on the orifice with stick representation of the cage except van-der-Waals spheres for the oxygen and hydrogen atoms of the orifice and the caged NO.

a RF pulse length of 25 μs. FSE data at a microwave frequency of 3.4 GHz (S band) were obtained again using a Bruker ElexSys E680 system with additional S band accessory including a Bruker Flexline probe head with a split-ring resonator employing a pulse timing of 32-500-64 ns. FSE and ENDOR spectra were fitted by the EasySpin (Stoll and Schweiger, 2006) "esfit" routine using the "pepper" and "salt" simulation routines.

2.3 Quantum chemical calculations

Optimization of the structure of the compounds NO@C60-OH1 and NO@C60-OH3 has been performed using Gaussian (g16-A03) at the HPC center of FU Berlin. DFT calculations were performed using the 6-311++ basis set with UB3LYP exchange. Structures derived for nitrogen in the "up" orientation (with respect to orifice) are depicted in Figs. 1 and A1. The difference in total energies for "up" and "down" orientations of the trapped radical was 22.6 meV for NO@C60-OH1, somewhat larger than the value (8 meV) published earlier (Hasegawa et al., 2018a), which might be caused by use of a different basis set. For NO@C60-OH3 we calculated 40.2 meV.

3 Results and Discussion

3.1 Multi-Frequency EPR Data

EPR data published previously by Hasegawa *et al.* for NO@C60-OH1 were obtained in continuous wave (cw) mode at a microwave frequency of 9.56 GHz (Hasegawa et al., 2018a). Spectra measured at 3.45 and 9.76 GHz using the FSE technique

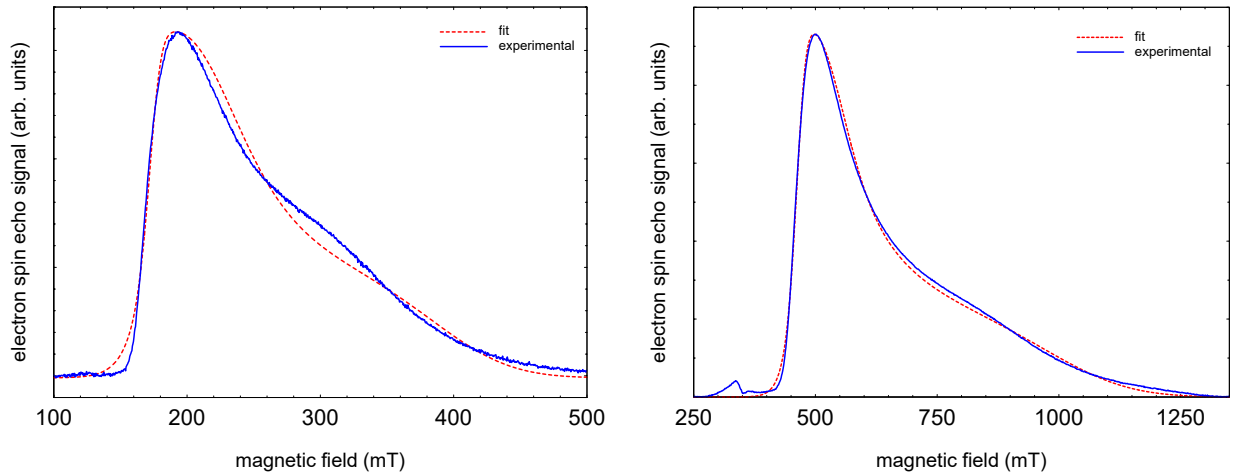

Figure 2. FSE spectra of NO@C60-OH1 ($T = 5$ K) with best fits. **Left:** S band (3.5 GHz, 10 mM/CS_2). **Right:** X band (9.7 GHz, 2.5 mM/CS_2). For fitting a set of nitrogen hyperfine tensor parameters was used, determined by ENDOR (see below).

Table 1. Fit-determined g matrix data of both compounds (gStrain fit parameters are listed in brackets). Previously published values (Hasegawa et al., 2018a) are given for comparison. Level splittings Δ deduced from the deviation of the pseudo-axial g_3 parameter from g_e are also shown.

sample	ν (GHz)	cw/FSE	g_1	g_2	g_3	Δ (meV)
NO@C60-OH1	3.45	FSE	1.438(0.007)	1.225(0.399)	0.646(0.134)	15.9
NO@C60-OH1	9.76	FSE	1.482(0.002)	1.350(0.275)	0.679(0.182)	16.9
NO@C60-OH3	3.45	FSE	1.480(0.012)	1.212(0.602)	0.725(0.129)	17.8
NO@C60-OH3	9.76	FSE	1.527(0.002)	1.422(0.287)	0.767(0.173)	19.7
NO@C60-OH1	9.57	cw	1.488	1.320	0.225	

are depicted in Fig. 2. The published g matrix parameter set (see Table 1) obtained by spectral simulation of the cw spectrum is characterized by an extreme g anisotropy. The values determined by fitting the FSE spectra confirm the two larger g matrix parameters, however deviate significantly with respect to the pseudo-axial g_3 parameter. We quote no error margins, because a large g strain value is obtained for the g_3 value using the "esfit" routine (EasySpin (Stoll and Schweiger, 2006)). The pseudo-axial principal parameter g_3 = 0.646 and 0.679, respectively, are still found to be very small compared to $g_3 = 1.7175$ for the same compound trapped in a crystal (Ryzhkov and Toscano, 2005) or $g_3 = 1.888$ when incorporated in a zeolite (Poeppl et al., 2000), but rendering the g matrix substantially less anisotropic compared to the data in ref. (Hasegawa et al., 2018a). For further confirmation of the g matrix parameter set determined by fitting the FSE spectra, we also performed a PEANUT experiment (Stoll et al., 1998), probing the Rabi nutation frequency as function of B_0 (see below).

Parameters determined for the NO@C60-OH3 compound are also listed in Table 1. Spectra are shown in Fig. A2 in appendix A. Also for this compound with slightly modified cage a similar set is observed, the fit parameters changing slightly towards larger

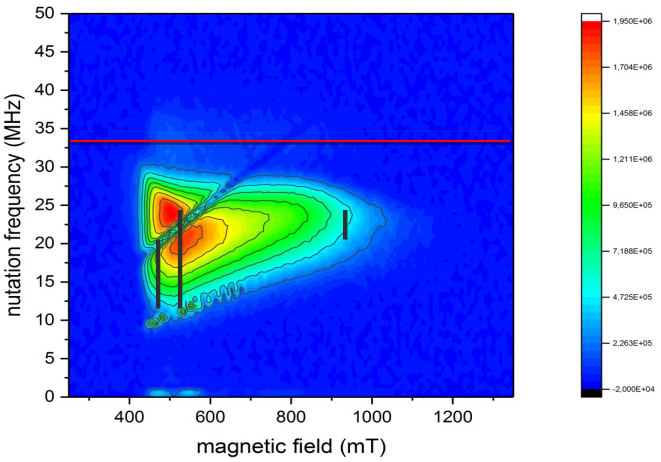

Figure 3. PEANUT spectrum of NO@C60-OH3 measured at 3.6 K. The red line indicates the reference frequency measured for a coal sample with isotropic $g = 2$. The black vertical lines indicate the expected nutation frequency distributions (Stoll et al., 1998) at the three principal g values for NO@C60-OH3 in Table 1 (X band).

values compared to those found for the OH1 compound. Even the slight difference in cage structure apparently is influencing the g matrix values. However, no prominent features of anticipated magnetic interaction between encapsulated NO radicals within the intermolecular hydrogen-bonded dimeric triply hydroxylated C_{60}-derived cages was observed.

Because of the rather large deviation of the g_i parameters from the free electron value and the large anisotropy of g, a significant variation of the nutation frequency was expected as function of orientation. If by orientation selection a particular g principal position is chosen, the two remaining g parameters determine the nutation frequency. As shown in Fig. 3, all Rabi frequencies are smaller than the reference value determined by a standard coal sample and increase towards the high field spectral range. In Fig. 3, the expected nutation frequency distributions (Stoll et al., 1998) are indicated by dashed vertical lines at the g principle values using the values for NO@C60-OH3 at X band in Table 1. The agreement is quite convincing, and a very small g_3 parameter as deduced earlier can be excluded, since it would lead to much smaller nutation frequencies down to ≈ 3.7 MHz in the perpendicular orientations (g_1 and g_2 region, 500 mT region) of the radical. Thus, the small value of g_3 = 0.225 (Hasegawa et al., 2018a) is probably caused by overestimating the flat high field part of the cw spectrum in the simulation.

It should be noted that the g matrix parameters of the encapsulated NO radical deviate much more from the free electron value g_e = 2.0023, compared to data reported for situations when the radical is either trapped in a crystal (g = (1.9740 (7), 1.9766 (7), 1.7175 (4))) (Ryzhkov and Toscano, 2005), adsorbed at the surface of metal oxides (g = (1.97, 1.97, 1.91)) (Lunsford, 1968), or incorporated in a zeolite (g = (2.001, 1.996, 1.888)) (Poeppl et al., 2000). This clearly indicates that the orbital momentum of the radical is much less quenched in the C_{60}-derived cages. Following the idea that partial quenching of the orbital angular momentum is caused by lifting of the degeneracy between the antibonding $^2\pi_x$ and $^2\pi_y$ orbitals, the energy splitting Δ between

these orbitals can be estimated by the pseudo-axial value of the NO g matrix (Ryzhkov and Toscano, 2005; Lunsford, 1968):

$$g_3 = g_e - 2\lambda L/(\lambda^2 + \Delta^2)^{1/2} \quad (1)$$

Here, λ is the spin-orbit coupling constant (123.16 cm^{-1} for NO (James and Thibault, 1964)), Δ defines the crystal-field splitting of the $^2\pi_x$ and $^2\pi_y$ orbitals, and L is a correction to the angular momentum along z caused by the crystal field. L is equal to 1 for a free molecule. A change in L represents a modification of the molecular wave function by the crystal field. It should be noted, however, that in previous studies (Zeller and Känzig, 1967; Shuey and Zeller, 1967) no significant deviations from 1 were observed. The highly nonlinear dependence of g_3 on Δ is depicted in Fig. A3 (appendix A). Using Eq. (1), a level splitting of approximately 17 meV (200 K) is determined from $g_3 \approx 0.7$ for NO@C60-OH1 and 20 meV from $g_3 \approx 0.8$ for NO@C60-OH3 (see Table 1). The lifting of the $^2\pi_x/^2\pi_y$ degeneracy is not unexpected considering the observation of a finite zero-field-splitting for $^3O_2$ in a cage with C_1 symmetry (Futagoishi et al., 2017). In this study the potential barrier for librational motions of $^3O_2$ was estimated as 398 cm^{-1} (49 meV), by measuring the shift of its principal ZFS component with respect to the value of the free molecule. The size of this potential barrier is of the same order of magnitude as the one calculated here for NO.

The lifting of degeneracy leads to a deviation of the orbitals from two fully circular symmetric angular momentum eigenstates with opposite momentum to two orthogonal elliptic orbitals not being angular momentum eigenstates, but with non-vanishing angular momentum expectation values. With a 200 K level splitting only one of the orbitals is occupied at 5 K and rotation of the molecule corresponds to transitions from one to the other eigenstate, which should be impossible due to the large level splitting. Nevertheless, the remaining angular momentum expectation value gives rise to the very small g_3 value. The splitting is much less than values found for ^{2}NO and $^2O_2^-$ trapped in crystals, on surfaces or in zeolites, which are ranging from 300 to 500 meV.

The $^2\pi_x$ and $^2\pi_y$ level splitting is of the same order of magnitude as the energy difference for the "up" and "down" orientation of the NO radical with respect to the cage opening calculated earlier (Hasegawa et al., 2018a) and also found in this study. For "up"/"down" axis reorientation a factor ten larger barrier was found. Considering the additional degree of freedom of hindered rotation about the axis of the radical with unknown transition barrier, this gives rise to a complicated 3-dimensional orthorhombic potential energy surface. It is not surprising that under these conditions the EPR signal can be detected only at very low temperatures. The temperature dependence of the NO FSE signal (X band) was measured relative to an unidentified stable $S = 1/2, g \approx g_e$ species in the sample and is shown in Fig. 4 left. The NO signal decreases much faster upon temperature increase than according to the Curie law since a dramatic signal loss relative to the reference signal is observed. This strong additional signal decay of the NO radical beyond the Curie law can be described by an activation temperature of about 3 K. The dramatic loss of signal intensity by a factor 50 in the narrow temperature range of 5 to 12 K is indicative for a decrease of T_2. This was confirmed by measuring the 2-pulse echo decay constant T_2^* at the peak signal position. Its temperature dependence could be fitted assuming exponential temperature dependence with an activation temperature of 3.1 K as shown in Fig. 4 right.

Measuring the field dependence of T_2^* at different temperatures, supports the simple model of a restricted rotation. As shown in Fig. 5 left, at 5 K the T_2^* values increase from 600 ns to 1500 ns, when probing radicals changing from perpendicular

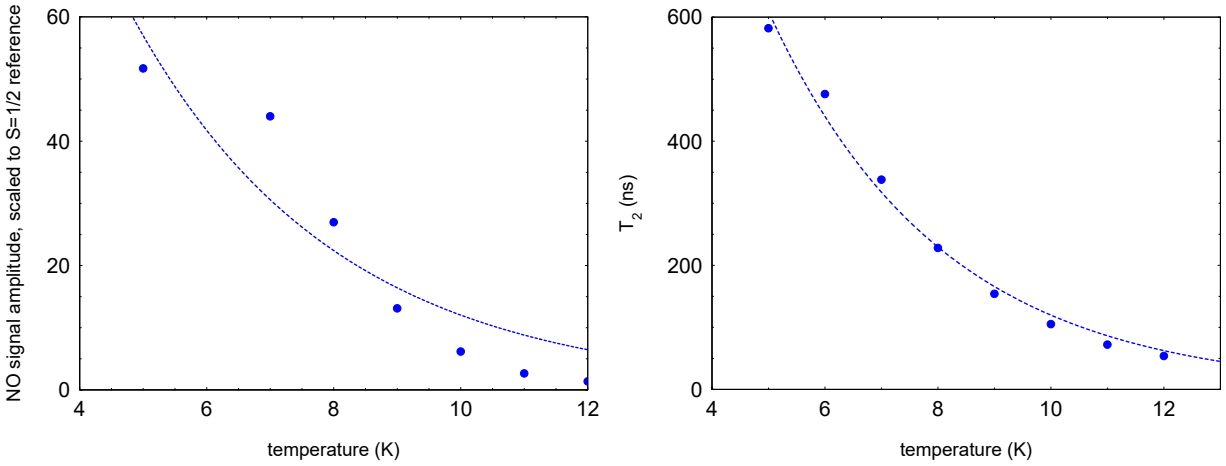

Figure 4. Echo-detected signal of NO@C60-OH3 (480 mT, 9.7 GHz, 2.5 mM/CS_2, 200 ns pulse separation) as function of temperature. The signal intensity is scaled to the intensity of a field separated $g \approx g_e$ signal from an unidentified $S = 1/2$ species following the Curie law. An exponential temperature dependence is assumed for the fit (dashed line) with a decay constant of 3 K. **Right:** Temperature dependence of the spin echo decay constant T_2 of NO@C60-OH3 (480 mT, 9.7 GHz, 2.5 mM/CS_2). The faster decay constant with larger weight is shown in cases where the time traces required a bi-exponential fit. Again an exponential temperature dependence is assumed for the dashed line, with a decay constant of 3.1 K.

to parallel orientation. This can be taken as evidence that small angle librations around the long axis are activated at this temperature, whereas long axis reorientations are still prevented at this temperature. In contrast, at 10 K this restriction is no longer valid, shortening the echo decay accordingly for the full field range, i.e. librations about all molecular axes occur.

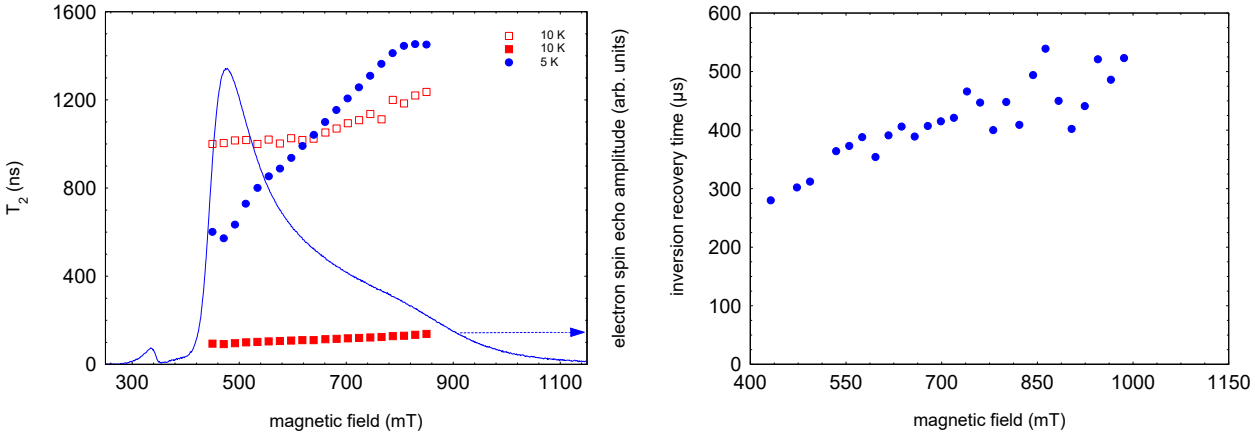

Figure 5. Left: Field and temperature dependence of 2-pulse echo decay of NO@C60-OH3. The 5 K data set could be satisfactorily fitted assuming a single exponential; the 10 K data required a bi-exponential fit. Both components were of similar magnitude, with the shorter T_2 larger in amplitude. **Right:** Field dependence of T_1 of NO@C60-OH3, measured using an inversion recovery pulse sequence at 3.6 K.

This hypothesis is also supported by the observation that T_1, determined by inversion recovery, also increases significantly at $T = 3.6$ K when moving from perpendicular to parallel orientation (see Fig. 5 right). This field dependence of T_1 leads even at 3.6 K to a noticeable change in the FSE pattern, if the pulse repetition time is not sufficiently long (see Fig. A4), appendix A). While as well T_1 as T_2 show a significant temperature dependence, the spectral shape, and thus the g parameters, are virtually unaffected within the temperature range of 3.6 to 12.5 K (see Table B1, appendix B).

Loss of the cw EPR signal intensity at temperatures above 80 K was also reported in ref. (Hasegawa et al., 2018b). Since the cw signal intensity is not affected by T_2^*, the NO signal could be detected in cw mode up to 40 K (Hasegawa et al., 2018b) with a much smaller decrease from 5 K to 20 K than observed in our pulsed EPR study probing the echo signal with a 2-pulse sequence. The low activation temperature of 3 K (~0.3 meV) has to be compared to the much larger values found in the case of N@C_{60}, and P@C_{60}, in which a well-defined potential of spherical or axial symmetry leads to degenerate vibrational levels of the translational degree of freedom of encapsulated atoms in the range of 8 to 16 meV (Pietzak et al., 2002), respectively. The partially opened cage resembles more the situation in the C_{70} cage by providing a nearly axial potential. Assuming that vibration along this preferred axis is lowest in energy and taking into account the larger mass of the radical, a vibrational eigenfrequency of about 5 meV for the center of mass (CM) of the radical would be expected, which is still more than one order of magnitude larger than the experimental value. In contrast to encapsulated atoms, we have also to consider for the NO case a librational mode of the radical with respect to the cage axis. In a study of H_2 encapsulated in C_{60} or C_{70}, the eigenstates of H_2 were determined numerically by invoking the appropriate 5-dimensional potential surface, describing translational and rotational degrees of freedom (Xu et al., 2009; Mamone et al., 2013). Lacking numerical values for the potential surface in our more complicated case, it is only possible to estimate typical values for the librational mode by approximating the interconversion between "up"/"down" (its z axis) of the radical axis in a potential well of 80 meV (645 cm^{-1}) (Hasegawa et al., 2018a) as a torsional oscillator. Converting the 80 meV rotational barrier into a torsion spring constant for librations of $\kappa = 40$ meV and using $\omega = \sqrt{\kappa/\theta}$ with the moment of inertia θ of NO, we arrive at a characteristic mode energy for the libration of about 4 meV (about 40 K), which is substantially larger than the experimentally observed activation temperature. However, when including transverse degrees of freedom for axis reorientation, it is not unlikely that the characteristic mode energies might further be reduced towards the experimental value.

3.2 ENDOR Data

Orientation selective ENDOR spectra of NO@C60-OH1 were measured at 9.7 GHz. As depicted in Fig. 6 (left), the center of lines shifts towards higher frequency, when changing the observation field position from lowest to highest edges of the absorption pattern. The frequency position at the low field side of the spectrum and the magnitude of the shift is inconsistent with proton hfi but is indicative for a dominant dipolar ^{14}N hfi, allowing simple determination of A_i for the extreme field positions. For a determination of dipolar and quadrupolar hfi parameters observation field values at the low and high ends of the FSE spectrum were chosen, anticipating that g matrix and hfi tensor axes are collinear. Best ENDOR resolution is obtained at the low field edge, allowing determination of some hfi parameters by fitting, as shown in Fig. 6 (right).

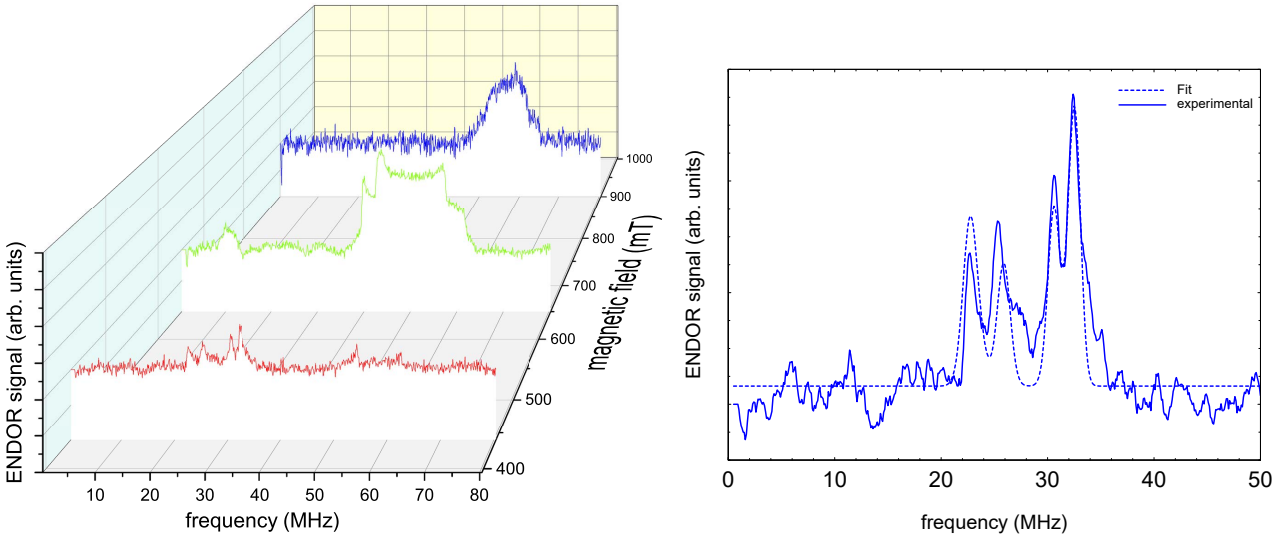

Figure 6. Left: Davies ENDOR spectra of NO@C60-OH1 ($T = 5$ K, 10 mM/CS_2) measured as function of B_0. Spectra are corrected with respect to different accumulation times for better comparison of spectral pattern. The Davies ENDOR pulse sequence (40-30000-20-200-40 ns, 25 μs rf pulse) was identical for all spectra. **Right:** ENDOR spectrum of NO@C60-OH1 measured at 440 mT (see left) together with simulation.

At this field position a consistent fit is obtained, by only fixing the nuclear Larmor frequency to its field-determined value. At the high field edge no line quartet is observed for this compound. The broad pattern, however, is consistent with the result of a spectral simulation, shown in Fig. 7, using a parameter set completed with the nqi parameter of NO@C60-OH3, being better resolved at the high-field edge of the ENDOR pattern. It should be noted that no simple pattern is expected for the intermediate field range because of significant g strain. For this reason fit values are only quoted assigned to g_1 and g_3 axes directions. No information about the signs of hfi parameters can be deduced from the experimental spectra. The assignments given in Table 2 are tentatively made by invoking the calculated hfi constants (see Table 3). Although not being in very good quantitative agreement with the experiment, the calculated small isotropic hfi ($+15$ MHz) necessitates assignment of a negative sign to A_1. Lacking spectral resolution when probing at the high field edge due to the large g_3 strain, the center of gravity still gives a reliable value for the large dipolar hfi for both compounds. The absent spectral resolution, even when observing at the van Hove singularities of the FSE spectrum could result from a simultaneous presence of "up"/"down" configurations as observed in X-ray crystallography, with slightly different hfi parameters.

Table 2. Hyperfine parameters determined by fitting Davies ENDOR spectra measured under orientation selection conditions providing best resolution. For an assignment of signs see text.

sample	A_1 (MHz)	A_2 (MHz)	A_3 (MHz)	Q_1 (MHz)	Q_2 (MHz)	Q_3 (MHz)
NO@C60-OH1	-55.3	N/A	+122.6	2.47	N/A	N/A
NO@C60-OH3	N/A	N/A	+124.1	N/A	N/A	1.1

Table 3. Hyperfine parameters calculated for NO@C60-OH1 and NO@C60-OH3 in their "up" configuration using Gaussian G16/A03 (G16/A03, B3LYP, 6-311++). The calculated values for the "down" orientation differ by less than 3%.

sample	A_1 (MHz)	A_2 (MHz)	A_3 (MHz)	Q_1 (MHz)	Q_2 (MHz)	Q_3 (MHz)
NO@C60-OH1	-25.5	-23.5	+90.2	-1.48	+0.22	+1.26
NO@C60-OH3	-25.4	-23.1	+90.5	-1.48	+0.22	+1.26

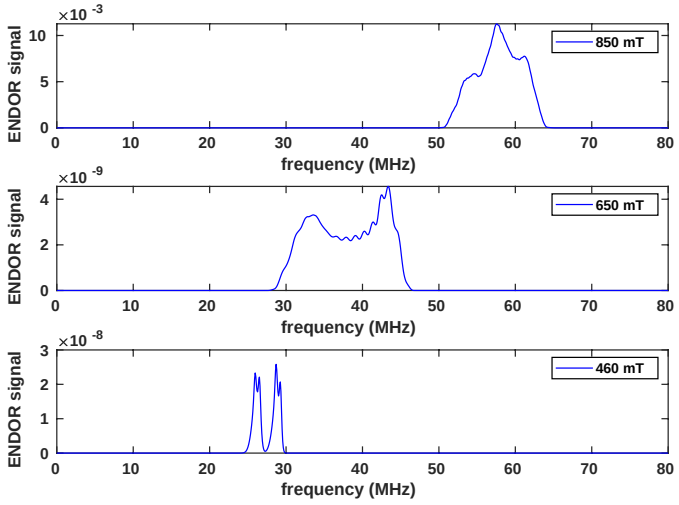

Figure 7. Simulated ENDOR spectra of NO@C60-OH1, using parameters listed in Table 2.

4 Conclusions

Using various EPR techniques, the spin Hamiltonian parameters for the encapsulated NO radical are determined. The radical, being confined in C_{60} derived cages, exemplifies the transition between a free molecule in isotropic potential and being fixed by a rigid confinement. The NO radical is particularly suited for such an investigation, since the g factor of the free molecule in its $^2\Pi_{1/2}$ rotational ground state will change between zero (Mendt and Pöppl, 2015) to a g matrix, in with all parameters are close to the free electron value for the rigidly localized radical (Chiesa et al., 2010). In case the axial molecular symmetry

is maintained by the environment allowing free rotation about its axis, the g parameter g_3, being assigned to the NO bond axis is predicted to vanish. The measured value g_3 = 0.77(5) is indicative for an intermediate situation of the radical and yields information about the locking potential's deviation from axial symmetry. This 17 meV asymmetry as found here is quite small compared to the situation in polycrystalline or amorphous matrices ranging from 300 to 500 meV. The analysis of the spin relaxation times resulted in an activation temperature of about 3 K, assigned to temperature activated motion of the radical with coupled rotational and translational degrees of freedom in the complicated 3-dimensional potential provided by the cage.

Performing ENDOR the ^{14}N hyperfine coupling parameters were determined. The experimental values are in fair agreement with predictions from a DFT calculation. The spectral resolution was not sufficient to discriminate between parameter sets expected for the Xray crystallography confirmed "up"/"down" configurations of the radical with respect to the orifice of the cage.

The g matrix parameters did not show any temperature dependence in the range of 3.6 to 12 K, in which a dramatic orientation dependent decrease of T_2^* is observed. This indicates that the radical is localized, not allowing for excitation of rotational modes about its axis, which would modify the g_3 value. Apparently only low energy modes with small amplitude around its equilibrium orientation are excited at these temperatures. It should be noted, however, that the accuracy of the data analysis is high enough to detect a small difference in g parameters using cages with slightly modified orifices. It will be interesting to see in the future, if advanced computational methods will be able to reproduce g matrix and hfi tensor data for this radical in such a complicated potential.

Code and data availability. Experimental data used for the figures and further information will be made available upon request for reviewing and uploaded to the refubium.fu-berlin.de institutional repository prior to publication.

Appendix A: Supplementary Figures

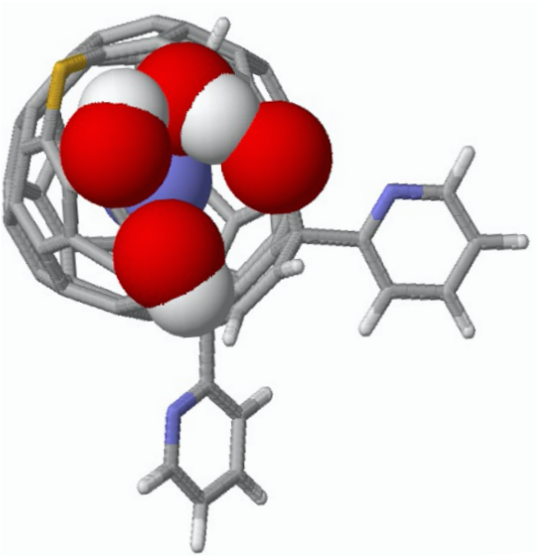

Figure A1. Top view on the DFT optimized structure of NO@C60-OH3 with N "up". The modified C_{60} cage is represented by sticks except van-der-Waals spheres for the oxygen and hydrogen atoms of the orifice and the caged NO (C (grey), H (white), N (blue), O (red), and S (yellow)).

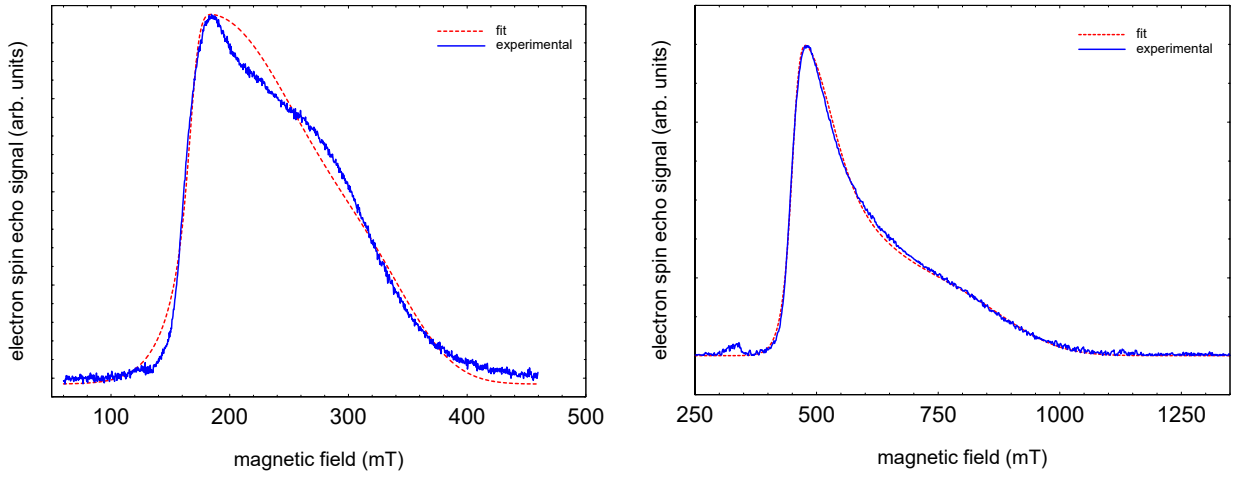

Figure A2. FSE spectra of NO@C60-OH3 (T = 5 K) with best fits. **Left:**S band (3.5 GHz, 10 mM/CS_2). **Right:** X band (9.7 GHz, 2.5 mM/CS_2)

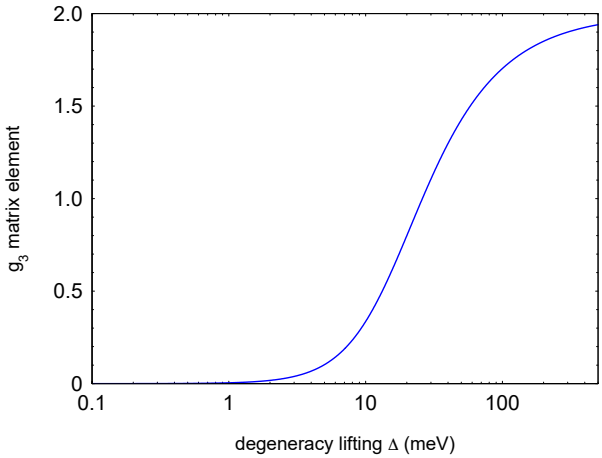

Figure A3. Dependence of the pseudo-axial g_3 matrix element of the NO radical as function of ${}^2\pi_x^*$ and ${}^2\pi_y^*$ level splitting.

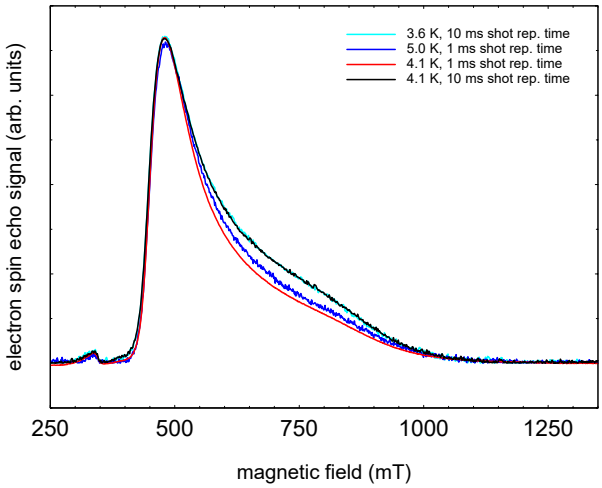

Figure A4. 9.7 GHz FSE spectra of NO@C60-OH3 measured at 3.6, 4.1, and 5 K. Using a rather short pulse repetition time (1 ms), the high-field part of the spectrum is partially saturated.

Appendix B: Supplementary Table

Table B1. Best fit parameters for the NO@C60-OH3 spectra measured at different temperatures (data not shown).

	g_1	g_2	g_3	g_1 strain	g_2 strain	g_3 strain	linewidth (mT)
5 K, 120 ns	1.527	1.422	0.767	0.002	0.294	0.171	17.4
10 K, 120 ns	1.521	1.420	0.717	0.001	0.348	0.131	12.6
10 K, 300 ns	1.505	1.419	0.699	0.001	0.432	0.139	13.2

Author contributions. Compounds were synthesized by SH, YH, and YM. EPR experiments were performed by KPD, TK, and RB. Data analysis was performed by KPD and RB, and the manuscript written by KPD with input from all authors.

Competing interests. The authors declare no competing interests

Acknowledgements. The authors thank Claudia Tait for very helpful discussions and the HPC Service of ZEDAT (Freie Universität Berlin) for computing time.

References

Bloodworth, S., Sitinova, G., Alom, S., Vidal, S., Bacanu, G. R., Elliott, S. J., Light, M. E., Herniman, J. M., Langley, G. J., Levitt, M. H., and Whitby, R. J.: First Synthesis and Characterization of CH4@C-60, Angewandte Chemie International Edition, 58, 5038–5043, 2019.

Chiesa, M., Giamello, E., and Che, M.: EPR Characterization and Reactivity of Surface-Localized Inorganic Radicals and Radical Ions, Chemical Reviews, 110, 1320–1347, 2010.

Futagoishi, T., Aharen, T., Kato, T., Kato, A., Ihara, T., Tada, T., Murata, M., Wakamiya, A., Kageyama, H., Kanemitsu, Y., and Murata, Y.: A Stable, Soluble, and Crystalline Supramolecular System with a Triplet Ground State, Angewandte Chemie International Edition, 56, 4261–4267, 2017.

Hasegawa, S., Hashikawa, Y., Kato, T., and Murata, Y.: Construction of a Metal-Free Electron Spin System by Encapsulation of an NO Molecule Inside an Open-Cage Fullerene C60 Derivative, Angewandte Chemie International Edition, 57, 12 804–12 808, 2018a.

Hasegawa, S., Hashikawa, Y., Kato, T., and Murata, Y.: supporting information, Angewandte Chemie International Edition, 57, 12 804–12 808, 2018b.

Hashikawa, Y., Hasegawa, S., and Murata, Y.: A single but Hydrogen-bonded water molecule confined in an anisotropic subnanospace, Chemical Communications, 54, 13 686–13 689, 2018.

James, T. C. and Thibault, R. J.: Spin—Orbit Coupling Constant of Nitric Oxide. Determination from Fundamental and Satellite Band Origins, The Journal of Chemical Physics, 41, 2806–2813, 1964.

Komatsu, K., Murata, M., and Murata, Y.: Encapsulation of Molecular Hydrogen in Fullerene C60 by Organic Synthesis, Science, 307, 238–240, 2005.

Krachmalnicoff, A., Bounds, R., Mamone, S., Alom, S., Concistre, M., Meier, B., Kouril, K., Light, M. E., Johnson, M. R., Rols, S., Horsewill, A. J., Shugai, A., Nagel, U., Room, T., Carravetta, M., Levitt, M. H., and Whitby, R. J.: The dipolar endofullerene HF@C-60, Nature Chemistry, 8, 953–957, 2016.

Kurotobi, K. and Murata, Y.: A Single Molecule of Water Encapsulated in Fullerene C60, 333, 613–616, 2011.

Lunsford, J. H.: Surface interactions of zinc oxide and zinc sulfide with nitric oxide, Journal of Physical Chemistry, 72, 2141–2144, 1968.

Mamone, S., Concistre, M., Heinmaa, I., Carravetta, M., Kuprov, I., Wall, G., Denning, M., Lei, X., Chen, J. Y., Li, Y., Murata, Y., Turro, N. J., and Levitt, M. H.: Nuclear magnetic resonance of hydrogen molecules trapped inside C70 fullerene cages, ChemPhysChem, 14, 3121–3130, 2013.

Mendt, M. and Pöppl, A.: The Line Width of the EPR Signal of Gaseous Nitric Oxide as Determined by Pressure and Temperature-Dependent X-band Continuous Wave Measurements, Applied Magnetic Resonance, 46, 1249–1263, 2015.

Murphy, T. A., Pawlik, T., Weidinger, A., Höhne, M., Alcala, R., and Spaeth, J.-M.: Observation of Atomlike Nitrogen in Nitrogen-Implanted Solid C60, Physical Review Letters, 77, 1075–1078, 1996.

Pietzak, B., Weidinger, A., Dinse, K.-P., and Hirsch, A.: Group V Endohedral Fullerenes: N@C60, N@C70, and P@C60, pp. 13–65, Kluwer Academic Publishers, The Netherlands, 2002.

Poeppl, A., Rudolf, T., Manikandan, P., and Goldfarb, D.: W- and X-Band Pulsed Electron Nuclear Double-Resonance Study of a Sodium-Nitric Oxide Adsorption Complex in NaA Zeolites, Journal of the American Chemical Society, 122, 10 194–10 200, 2000.

Rübsam, M., Schweitzer, P., and Dinse, K.-P.: Rotational dynamics of metallo-endofullerenes in solution, Journal of Physical Chemistry, 100, 19 310–19 314, 1996.

Ryzhkov, L. R. and Toscano, J. P.: Crystal Lattice Effects on the Orientation and Orbital Degeneracy of Nitric Oxide Trapped in Nitramine Single Crystals, Crystal Growth & Design, 5, 2066–2072, 2005.

Saunders, M., Jiménez-Vázquez, H. A., Cross, R. J., Mroczkowski, S., Gross, M. L., Giblin, D. E., and Poreda, R. J.: Incorporation of Helium, Neon, Argon, Krypton, and Xenon into Fullerenes using High Pressure, Journal of the American Chemical Society, 116, 2193–2194, 1994.

Shuey, R. T. and Zeller, H. R.: Die elektronische Struktur des $^2O_2^-$-Zentrums in den Alkalihalogeniden II. Theoretische Betrachtungen, Helvetica Physica Acta, 40, 873–886, 1967.

Stevenson, S., Rice, G., Glass, T., Harich, K., Cromer, F., Jordan, M. R., Craft, J., Hadju, E., Bible, R., Olmstead, M. M., Maitra, K., Fisher, A. J., Balch, A. L., and Dorn, H. C.: Small-bandgap endohedral metallofullerenes in high yield and purity, Nature, 401, 55–57, 1999.

Stoll, S. and Schweiger, A.: A comprehensive software package for spectral simulation and analysis in EPR, Journal of Magnetic Resonance, 178, 42–55, 2006.

Stoll, S., Jeschke, G., Willer, M., and Schweiger, A.: Nutation-Frequency Correlated EPR Spectroscopy: The PEANUT Experiment, Journal of Magnetic Resonance, 130, 86–96, 1998.

Xu, M., Sebastianelli, F., Gibbons, B. R., Bacic, Z., Lawler, R., and Turro, N. J.: Coupled translation-rotation eigenstates of H_2 in C60 and C70 on the spectroscopically optimized interaction potential: Effects of cage anisotropy on the energy level structure and assignments, The Journal of Chemical Physics, 130, 224 306, 2009.

Zeller, H. R. and Känzig, W.: Die elektronische Struktur des $^2O_2^-$ Zentrums in den Alkalihalogeniden I. Die paramagnetischen und optischen Spektren und ihre Interpretation, Helvetica Physica Acta, 40, 845–872, 1967.